Journal of Membrane Science 619 (2021) 118747

Contents lists available at ScienceDirect

Journal of Membrane Science

journal homepage: http://www.elsevier.com/locate/memsci

# In-situ monitoring of polyelectrolytes adsorption kinetics by electrochemical impedance spectroscopy: Application in fabricating nanofiltration membranes via layer-by-layer deposition

Yuanzhe Liang [a,b,1], Fei Gao [c,d,1], Li Wang [a], Shihong Lin [a,b,e,*]

[a] Department of Civil and Environmental Engineering, Vanderbilt University, Nashville, TN, 37235, United States
[b] Interdisciplinary Material Science Program, Vanderbilt University, Nashville, TN, 37235, United States
[c] State Key Laboratory of Separation Membranes and Membrane Processes, Tianjin Polytechnic University, Tianjin, 300387, China
[d] School of Environmental Science and Engineering, Tianjin University, Tianjin, 300072, China
[e] Department of Chemical and Biomolecular Engineering, Vanderbilt University, Nashville, TN, 37235, United States

ARTICLE INFO

*Keywords:*
Layer-by-Layer
Adsorption
Electrochemical impedance spectroscopy
Nanofiltration

ABSTRACT

We herein report a novel approach based on electrochemical impedance spectroscopy (EIS) for in-situ monitoring of the adsorption kinetics in preparing polyelectrolyte multilayer nanofiltration membranes using layer-by-layer (LbL) deposition. Unlike existing methods for monitoring adsorption kinetics, this new approach is non-destructive and applicable to various substrates (as it does not use the substrate as a sensor). The model nanofiltration membrane used in this study is prepared by alternate depositions of Poly(diallyldimethylammonium chloride) and Poly(sodium 4-styrenesulfonate) on a polyacrylonitrile ultrafiltration membrane as the support. In each deposition step, the EIS measurements yield two important parameters, including the interfacial layer solution resistance and the film resistance, for probing the extent of polyelectrolyte deposition and membrane performance. The extent of polyelectrolyte deposition as probed by the EIS measurements is well corroborated by independent measurements of the membrane surface potential and the nanofiltration performance including water permeability and $Na_2SO_4$ rejection. This EIS-based approach enables the optimization of membrane fabrication using LbL deposition by conveniently identifying the minimum deposition time required to attain surface saturation.

## 1. Introduction

Nanofiltration (NF) is a membrane-based solute and molecular separation process that has been playing an increasingly important role in water treatment and wastewater reclamation [1–7]. It is a low-pressure membrane process with separation performance between reverse osmosis (RO) and ultrafiltration (UF) [8–10]. Unlike RO membrane that rejects almost all solutes from the feed solution, NF membranes typically have a comparatively loose active layer that partially rejects large ions and small organic molecules. The selectivity of NF membrane is mainly dependent on the pore size and the surface charge [11,12]. In general, NF membranes retain solute larger than the pore size and/or with charge similar to the surface and pore of the membrane [13,14].

Most existing commercial NF membranes are thin-film-composite polyamide (TFC-PA) membranes fabricated via interfacial polymerization (IP) [8–10]. Although polyamide-based NF membranes exhibit excellent perm-selectivity in many NF applications, they suffer from the propensity to organic and biological fouling and the poor chlorine resistance that prohibits aggressive membrane cleaning, which results in increased energy consumption in long-term operation and a relatively short membrane lifetime [15–18]. As an alternative to IP, Layer-by-Layer (LbL) deposition has been actively explored to fabricate membranes with polyelectrolyte multilayer (PEM) active layer. Over the last few decades, fabrication of PEM-nanofiltration (PEM-NF) membranes using LbL deposition has received growing interests due to its vast potential for tuning NF membrane performance with fine control of active layer film properties [19–24]. These features allow for engineering functional PEM-NF membranes with excellent fouling resistance and chemical stability in harsh conditions [25–28].

Typically, a PEM-NF membrane is formed by electrostatic self-

* Corresponding author. Department of Civil and Environmental Engineering, Vanderbilt University, Nashville, TN, 37235, United States.
*E-mail address:* shihong.lin@vanderbilt.edu (S. Lin).
[1] These authors contribute equally to this work.

https://doi.org/10.1016/j.memsci.2020.118747
Received 4 July 2020; Received in revised form 26 August 2020; Accepted 14 September 2020
Available online 2 October 2020
0376-7388/© 2020 Elsevier B.V. All rights reserved.

assembly of two oppositely charged polyelectrolytes [29,30]. The kinetics of adsorption of polyelectrolytes onto an oppositely charged surface is primarily regulated by diffusion and charge overcompensation [20,31–33]. Many competing factors affect the kinetics of polyelectrolyte adsorption, including polyelectrolyte type (e.g., strong or weak polycations vs. polyanions), molecular weight, concentration, substrate charge density, and the presence of inert, non-adsorbing electrolytes [31]. Studying the impacts of these factors on polyelectrolyte deposition and optimizing NF membrane synthesis based on LbL deposition requires an effective approach for monitoring the kinetics of polyelectrolyte adsorption. An ideal method for probing the kinetics of polyelectrolyte adsorption in NF membrane fabrication should be in-situ, non-interfering with the membrane fabrication process, and does not require the use of special substrates as sensors.

Unfortunately, existing approaches of monitoring adsorption kinetics fail to satisfy all these requirements. These methods include UV/Vis spectroscopy [34,35], small-angle X-ray scattering [36], quartz crystal microbalance with dissipation (QCM-D) [37,38], conductometric and potentiometric titration [39], ion-sensitive field-effect sensors and transistors [40]. While these techniques can provide useful information about polyelectrolyte deposition, each of them has their respective limitations. For instance, UV/Vis spectroscopy can only be applied to polyelectrolytes with optically sensitive functional groups [34]. Conductometric and potentiometric titrations require the presence of titratable functional groups in the polyelectrolyte species. X-ray scattering is a powerful tool to characterize the change of the film thickness, but provides limited information on adsorption kinetics [17]. QCM measurements can only be performed using piezoelectric crystal, which limits the choices of adsorption substrates and cannot be applied in real membrane fabrication processes [37]. A similar limitation also applies to methods based on ion-sensitive field-effect sensors and transistors [40].

Electrochemical impedance spectroscopy (EIS) is a powerful technique with diverse applications in studying reactions and interfacial processes, including corrosion [41], coatings [42], electrocatalytic reactions [43], and redox reactions [44]. Efforts have been made to analyze the adsorption of polyelectrolyte onto a modified electrode, which provides insights into the growth kinetics of PEM films [45,46]. In those studies, the application of EIS was limited to studying PEM grown on special substrates, such as silicon and quartz electrodes. However, it remains challenging to directly study the kinetics of adsorption on porous membranes to monitor the growth of PEM in real membrane fabrication processes.

Here, we report a novel technique based on a four-electrode EIS system for studying the kinetics of polyelectrolyte adsorption onto a porous support in the context of fabricating PEM nanofiltration (NF) membrane. This technique represents an in-situ and non-destructive method for monitoring the growth of the PEM forming on a membrane substrate via LbL deposition. Specifically, we use a model system comprising poly (diallyldimethylammonium chloride) (PD) as the polycations, and poly (sodium 4-styrene sulfonate) (PS) as the polyanions. This model system has been widely investigated for preparing PEM-NF membranes via LbL deposition [24,47]. We perform EIS measurements during the sequential depositions of the six layers of polycations and polyanions on a polyacrylonitrile (PAN) ultrafiltration membrane and extract the solution resistance and charge transfer resistance from the EIS spectra. Finally, we characterize the PEM-NF membranes with different adsorption time and correlate the membrane properties and NF performance with the characteristics of the adsorption process.

## 2. Materials and methods

### 2.1. Materials and chemicals

Polyacrylonitrile (PAN) ultrafiltration membrane (MWCO = 50 kDa, GE Healthcare Life Science) was used as the substrate for fabricating the PEM-NF membrane. Poly(diallyldimethylammonium chloride) solution (PD, 25%, 400–500 kDa), Poly(sodium 4-styrenesulfonate) (PS, 1000 kDa), hydrochloric acid (HCl, ACS reagent, 37%), sodium hydroxide (NaOH, Bioxtra, ≥ 98%) and $Na_2SO_4$ (≥99%), were purchased from Sigma-Aldrich (St. Louis, MO US). All chemicals were used as received without further purification. Deionized water (Millipore, US) was used to prepare polyelectrolyte solutions and surfactant solution.

### 2.2. Fabrication of PEM-NF membrane

The PEM-NF membrane was prepared by depositing PD and PS alternately onto a PAN ultrafiltration (UF) membrane (the chemical structures of PD and PS are shown in Fig. 1). The PAN-UF membrane was first treated with a 2 mol $L^{-1}$ NaOH solution for 30 min to acquire negative surface charge, then immersed into DI water to remove excess NaOH, and finally dried in the oven before use. The hydrolyzed PAN membrane was exposed to the polycation solution (2 g $L^{-1}$ PD), rinsed with DI water, then exposed to a polyanion solution (2 g $L^{-1}$ PS), and finally rinsed with DI water. The resulting membrane is referred to as the $(PD\text{-}PS)_1$ with the subscript "1" representing one PD-PS bilayer. The same procedure was repeated to form additional bilayers, $(PD\text{-}PS)_2$ and $(PD\text{-}PS)_3$.

### 2.3. EIS measurement, equivalent circuit, and parameters extraction

In each polyelectrolyte deposition step, EIS measurement was performed using a potentiostat (SP-150 BioLogic, France) equipped with a custom-made EIS cell (Fig. 1A, also Supplementary Fig. 1). The cell dimension is 80 mm × 80 mm × 80 mm with an effective membrane area of 4.52 $cm^2$. The cell consists of two chambers, each containing an electrode for injecting current (the working electrode and counter electrode) and an electrode for measuring the potential across the membrane (the working sense electrode and the reference electrode) [48]. The polycation and polyanion solutions were alternately introduced to the PAN substrate in a non-flow electrochemical cell, and the process of polyelectrolyte deposition was in-situ monitored. The four-electrode system separates the measurements of current and voltage, and thereby eliminates the complicating effects of the frequency-dependent impedance at the interface between the solution and the working electrode.

This setup, shown in Fig. 1A and B, enables the simultaneous measurements of solution resistance near the solution-membrane interface and the film resistance without mutual interference. The working and counter electrodes are responsible for current injection, whereas the working sense and reference electrodes are for measuring potential difference across the PEM. The working electrode is a platinum ring placed in the polyelectrolyte solution, whereas the counter electrode is a platinum foil placed in the polyelectrolyte-free solution on the opposite side of membrane. The working sense electrode and the reference electrode are two platinum wires placed in direct contact of the two sides of the substrate membrane, respectively. The direct contact of the working sense electrode and the reference electrode with the membrane is critical to the measurement consistence, whereas the use of wires (instead of foil) minimizes the interference of the electrodes with the polyelectrolyte deposition.

The input was a sinusoidal perturbation signal with an amplitude of 10 mV (vs. the open-circuit potential). Unless specified, an impedance spectrum was recorded every 120s with a sweep frequency from 50 kHz to 0.1 Hz. However, we also performed some EIS measurements only within the high frequency range to shorten the scan time to extract the early stage evolution of certain parameters. Each polyelectrolyte deposition experiment was repeated for three times and the average and standard deviation of the parameters extracted from the EIS measurements are reported. Fitting of the impedance data was performed using commercial software, ZView®.

The EIS spectra were modeled using a $R_i$-($R_m$/Q) equivalent circuit

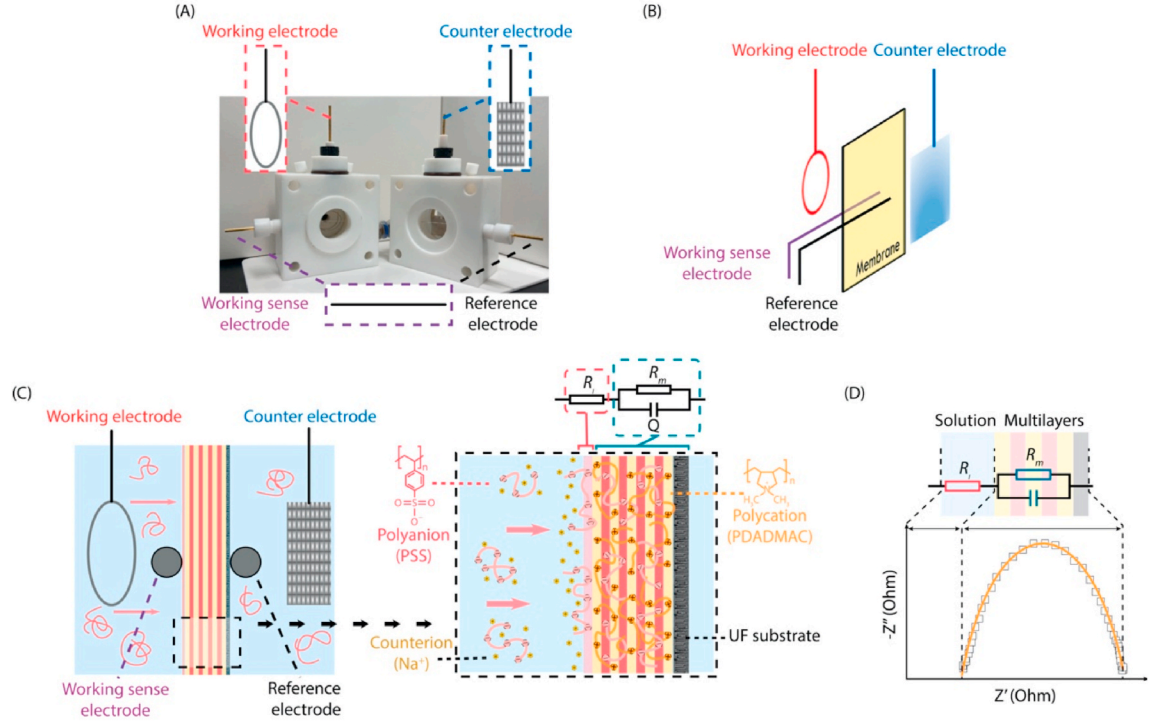


**Fig. 1.** **(A)** A custom-made EIS cell for EIS measurements. **(B,C)** Schematic illustration of the electrodes' positions in the EIS measurements. The $R_i$-($R_m$/Q) equivalent circuit used to fit the EIS spectra. The equivalent circuit comprises a parallel circuit $R_m$/CPE connected in series to a resistance $R_i$. **(D)** Illustration of Nyquist plot of the measured impedance and its interpretation using the equivalent circuit. The intercept of the x-axis represents the interfacial solution layer resistance, $R_i$. The film resistance $R_m$, and the non-ideal capacitive behavior, Q, are related to the size of the semi-circle.

connecting a resistance $R_i$ with an RC circuit of $R_m$/Q (Fig. 1C) [49]. Specifically, $R_i$ stands for the interfacial solution resistance which is the resistance of a thin film of solution near the membrane surface. The value of this resistance primarily depends on the abundance of the counter ions of the immobilized polyelectrolyte, and is thus closely related to the surface charge of the membrane [50,51]. $R_m$ represents the film resistance corresponding to the diffusion resistance of mobiles ions across the PEM-NF membrane [49,52–55]. Lastly, $Q$ represents the constant phase element (CPE) accounting for the non-ideal capacitive behavior. In the EIS spectrum, $R_i$ is the first x-intercept in the Nyquist plot, while $R_m$ and Q relate to the size of the semi-circle. Confidence limits of the best-fit model parameters were quantified by evaluating the variance-covariance matrices of the Levenberg-Marquardt algorithm employed in a non-linear $R^2$ minimization between the model and data [56].

While the interfacial electrochemical adsorption has been extensively studied for electrodes and functionalized conductive substrates using three-electrode systems [51,56], a three-electrode system does not enable direct characterization of the adsorption of charged species to a dielectric such as a membrane. This challenge is overcome in our four-electrode system where a pair of electrodes for measuring potential difference are attached to the two sides of the membrane to detect the subtle potential difference when electrostatic adsorption occurs at the solution-membrane interface. Despite the large resistance from the membrane substrate, the four-electrode system was sufficiently sensitive to detect the slight change of interfacial solution resistance ($R_i$) and film resistance ($R_m$) related to polyelectrolyte deposition. These two parameters extracted from the EIS spectra following the equivalent circuit model provide useful insights into understanding the process of LbL deposition.

### 2.4. NF membrane characterization and performance testing

As charge overcompensation is the primary driving force of polyelectrolyte adsorption, the change of surface charge density or potential is an important indicator of the adsorption progress. We prepared the $(PD\text{-}PS)_n$ (n = 1,2,3) membranes with different adsorption time, ranging from 0 to 60 min, for the adsorption of the PS top-layer onto underlying polyelectrolyte multilayers (capped with PD before PS adsorption). Except for this top layer of PS for which we intentionally varied the adsorption time, each layer of the underlying polyelectrolyte was prepared with a 30 min deposition time. The $\zeta$-potentials of the $(PD\text{-}PS)_n$ membranes with different top-layer PS adsorption time were determined by streaming current measurements using a streaming potential analyzer (SurPASS electro-kinetic analyzer, Anton Paar, Ashland, VA) with an adjusting gap cell with a channel width around 100 μm and 1 mM KCl solution as the background electrolyte. The zeta potential is calculated according to the method by Helmholtz-Smoluchowski [57]:

$$\zeta = \frac{dI}{dp}\frac{\eta}{(\varepsilon - \varepsilon_0)}\frac{L}{A}$$

where $\zeta$ is the zeta potential, $dI/dp$ is the slope of streaming current vs. differential pressure, $\eta$ is the dynamic viscosity of the liquid, $\varepsilon$ is the dielectric coefficient of solvent, $\varepsilon_0$ is vacuum permittivity, $L$ is the length of the streaming channel and $A$ is the cross-section of the streaming channel. We note that while the charged porous substrate may have impacts on the measured zeta potential [58–60], this effect is difficult to quantify due to the technical challenge of accurately distinguishing the properties of the active layer and the PEM. However, relative change of surface zeta potential of the PEM would not be affected without considering the impact of the substrate porosity.

NF performance of the $(PD\text{-}PS)_n$ (n = 1,2,3) membranes with different adsorption time was evaluated using a cross-flow filtration cell with an active membrane area of 7.1 $cm^2$. The pure water permeability of the $(PD\text{-}PS)_n$ membranes was evaluated using DI water. The crossflow velocity was 0.62 m $s^{-1}$ and the applied pressure was 2 bar. We evaluated the rejection of $Na_2SO_4$ (1 g $L^{-1}$), which is commonly used in NF

performance testing. The salt concentrations of the feed and permeate solutions were determined by measuring the electrical conductivity of the solutions with a calibration curve. The pure water permeability of the NF membrane was defined using the following equation:

$$PWP = \frac{J}{\Delta P}$$

where *PWP* is the pure water permeability of the NF membrane (unit: L $m^{-2}$ $h^{-1}$ $bar^{-1}$), $J$ is the volumetric flux of water (unit: L $m^{-2}$ $h^{-1}$), and $\Delta P$ was the applied pressure (unit: bar), respectively. The solute rejection, $R$, is calculated using the following equation:

$$R = \left(1 - \frac{c_p}{c_f}\right) \times 100\%$$

where $c_p$ and $c_f$ are the solute concentrations of permeate and feed solution, respectively.

## 3. Results and discussion

### 3.1. Evolution of interfacial solution and film resistances reflects polyelectrolytes growth

Both the interfacial solution resistance and film resistance changed throughout the adsorption process (Fig. 2). Each semi-circle represents a full EIS spectrum at a certain period in the adsorption process (Fig. 2A). The frequency of the spectrum scan ranged from 50 kHz to 0.1 Hz. The spectrum initially shifted to the right before shifting back toward the left as the polyelectrolyte deposition continued, which suggests that $R_i$ increased slightly at the beginning of the adsorption process due to the loss of mobile counterions in the interfacial layer and then gradually decreased as the mobile ions concentration restored (Fig. 2B). In comparison, the film resistance, $R_m$, which quantifies the diffusion resistance of mobile ions (counterions) across the PEM-NF membrane, monotonically increased as the adsorption process occurred and eventually approached a maximum (Fig. 2C). The increase in $R_m$ results from more difficult ion transport across the membrane as the PEM layer grows thicker. While more discussion will be provided later, the EIS data in Fig. 2 show that the temporal evolution of both interfacial solution resistance ($R_i$) and film resistance ($R_m$) reasonably reflects the dynamics of polyelectrolyte adsorption.

### 3.2. Time-dependent interfacial and film resistances during polyelectrolytes growth

Polyelectrolyte adsorption is a process driven by electrostatic interaction and limited by diffusion. In such a process, polyelectrolyte molecules first diffuse from the bulk solution to the interfacial layer near the membrane surface under a concentration gradient due to the consumptive adsorption, and then bind onto the charged substrate via electrostatic attraction. Upon contact with the PEM surface, a small segment of the polyelectrolyte chain is anchored onto the surface forming a large number of loops (segments with two anchor point on the PEM surface) and tails (segments with one anchor point on the PEM surface), while a large portion of segments still protrudes into the solution [34,61]. In a salt-free environment, the electrostatic attraction between two strong polyelectrolytes, e.g. PD and PS, leads to the spatial rearrangement of polyelectrolyte chain because the enthalpy reduction associated with the increased contact between the substrate and the polymer with a more extended configuration outweighs the corresponding loss of entropy [62].

Probing the $R_i$ extracted from EIS data provides useful information regarding the kinetics and extent of adsorption. The adsorption dynamics in each step is illustrated using the inverse of normalized interfacial resistance, defined as the ratio between the final interfacial resistance, $R_{i,f}$, and the real-time interfacial resistance, $R_i$, i.e., $R_{i,f}/R_i$ (Fig. 3A and Supplementary Fig. S2). The value of $R_{i,f}/R_i$ roughly quantifies the real-time abundance of counter ions on the membrane surface as compared to that at adsorption equilibrium, as $1/R_i$ positively correlates to the abundance of counter ions.

Instead of scanning the full frequency range, we performed partial spectrum scans only in the high-frequency range (10 kHz–0.3 kHz) to shorten the time of each scan (Supplementary Fig. 3). For both PS adsorption onto PD-coated surfaces and PD adsorption onto PS-coated surfaces, $R_{i,f}/R_i$ dropped slightly in the initial stage of adsorption (Fig. 3A), as the substrate surface became neutralized [63]. After this initial stage, $R_{i,f}/R_i$ continued to increase as the surface became increasingly overcharged. The increase of $R_{i,f}/R_i$ eventually leveled off as the adsorption approached completion. Comparing the adsorption of the two polyelectrolytes, we find that the initial-stage adsorption is faster for PD adsorption onto the PS-coated surfaces than for PS adsorption onto PD-coated surfaces, which is reflected by the earlier emergence of the minimum $R_{i,f}/R_i$ when PD adsorb onto the PS-coated surfaces.

The faster initial adsorption of PD can be explained by the much higher surface charge (in absolute value) of the PS-coated surface (Fig. 3B, negative values) than that of PD-coated surface (Fig. 3B, positive values). Therefore, the initial driving force for PD adsorption onto the PS-coated surface is much stronger than that for PS adsorption onto the PD-coated surface. In addition, the diffusion rate of PD (Mw~400–500 kDa) is estimated to be ~1.5 times larger than that of PS (Mw~1000 kDa) [64,65]. Consequently, the low adsorption rate of PS onto the PD-coated PEM surface and the low diffusion rate of PS from bulk solution to the membrane surface synergistically delayed the emergence of the $R_{i,f}/R_i$ minimum.

The initial $R_i$ value in each adsorption step throughout a sequential six-layer LbL deposition is shown in (Fig. 3C squares). The initial $R_i$ of the same type of surface decreased as more layers of polyelectrolytes were deposited, which is primarily due to the increase of (the absolute value) of the surface potential as a more strongly charged surface would bear more counter ions before adsorption. The change of interfacial

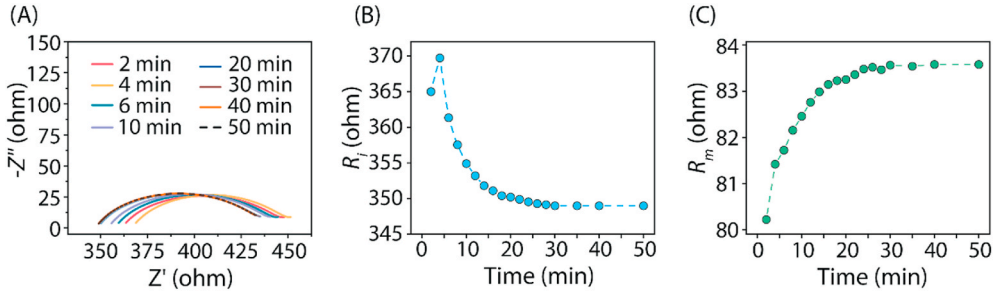


**Fig. 2.** **(A)** Example Nyquist plots of impedance of the solution near the solution-membrane interface and the polyelectrolyte active layer as a function of time during the deposition of the second PS layer onto the PAN-(PD-PS-PD) surface. **(B)** Change of solution resistance ($R_i$) as a function of time deduced from Nyquist plot. **(C)** Change of film resistance ($R_m$) as a function of time deduced from Nyquist plot.

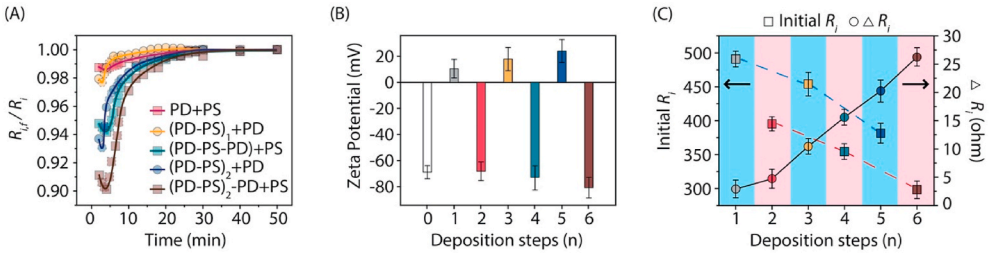


**Fig. 3. (A)** Temporal evolution of the inverse of the normalized interfacial resistance, $R_{i,f}/R_i$ at different deposition stages as extracted from EIS data (squares for PS adsorption onto a PD-coated surface and circle for PD adsorption onto a PS-coated surface). **(B)** Surface zeta potential of PEM-NF membranes with different layers of polyelectrolytes. The deposition time of each polyelectrolyte layer was 30 min. Error bars represent standard deviations of three replicate measurements. **(C)** Initial $R_i$ (before the new step of adsorption) and the change of $R_i$ for each deposition step.

solution resistance in each deposition step (i.e., the difference between final and initial $R_i$ of either a PS or PD deposition step), $\Delta R_i$, continued to grow with a larger number of deposited layers (Fig. 3C, circles). This implies that more polyelectrolytes deposit in the later steps of the LbL process, which is consistent with the growingly larger difference in zeta potential between two adjacent layers as the number of layers increased (Fig. 3B).

The EIS spectra also yield another important parameter, namely the film resistance ($R_m$), which quantifies the transmembrane diffusion resistance of mobile ions across the PEM-NF membrane. The resistance $R_m$ of a film is directly related to ionic permeability [49,52], and is dependent on surface charge, film thickness, and the ion diffusivity. The temporal variation of $R_m$ as extracted from fitting the equivalent circuit suggests that $R_m$ rapidly increased in the early stage of adsorption and gradually leveled off as adsorption approached completion (Fig. 4A). The increase in $R_m$ resulted from more difficult *trans*-membrane diffusion as the more polyelectrolyte accumulated on the membrane surface, and $R_m$ reached a maximum value when the polyelectrolyte adsorption ended due to saturation of surface adsorption site. In addition, the $R_m$ increased following an exponential function in the form of $1-\exp(-kt)$ and leveled off at the end of adsorption which also reflects the accumulation of polyelectrolyte on the PEM surface. Regardless of the adsorption step in the LbL deposition process, $R_m$ always reached a maximum at roughly 30 min. The adsorption time reflected by the temporal evolution of $R_m$ is highly consistent with that measured using the interfacial solution layer resistance, $R_i$(Fig. 3A).

Comparing the temporal evolution of $R_m$ at different deposition steps also reveals that $R_m$ increased slightly faster for polycation (PD) adsorption than for polyanion (PS) adsorption (Fig. 4A). The difference in the rates of $R_m$ increase is attributable to the fact that PS-coated membrane surfaces were more strongly charged whereas PD-coated surfaces had surface potentials that were closer to zero (Fig. 3B). Specifically, the fastest adsorption was observed with the positively charged PD adsorbing onto the membrane covered with $(PD\text{-}PS)_2$ which had the most negative charge among surfaces subject to further adsorption (no additional adsorption was performed beyond $(PD\text{-}PS)_3$ which was even more negative). The same conclusion could also be drawn from the PS adsorption: the adsorption rate increased with the number of polyelectrolyte layers.

The final values of $R_m$ also reveal important insights regarding the properties of the PEM layers. First, the final values of $R_m$ for the PD-capped film are systematically higher than that of the PS-capped film (Fig. 4B). This is likely because (1) the PD-capped surface is substantially less charged than the PS-capped surface (Fig. 3B) and (2) the counter anion for PD, $Cl^-$, has a substantially smaller Stoke radius (1.21 Å) as compared with that of the counter cations for PS, $Na^+$ (1.84 Å) [66]. Second, comparing the PEM-NF membranes of the same capping polyelectrolyte across different steps of deposition, $R_m$, increased systematically as the number of layers increased (Fig. 4B). Even though the absolute values of the surface potential increased (Fig. 3B), which tends to enhance ion permeability and thus reduces $R_m$, $R_m$ still increased systematically due to the increase of the PEM film thickness.

### 3.3. Correlating membrane property and performance with film resistance

Because observations from Figs. 3A and 4A suggest the effective time of the adsorption was consistently ~30 min regardless of the step in the LbL deposition, we hypothesize that the membrane property and performance depend on the polyelectrolyte adsorption time until it reaches 30 min. To test such a hypothesis, we fabricated a series of PEM-NF membranes with different PD-PS bilayers (1, 2, and 3 bilayers) with each surface layer obtained using different adsorption time (from 0 to 60 min). We note that the different adsorption time applies only to the top layer, whereas the underlying PEMs all have the same composition. Therefore, the membrane sample with 0-min adsorption time is a membrane with the complete underlying layers but not the top layer. Thirty membrane samples were fabricated following such an experimental design. The surface potential, water permeability, and rejection of $Na_2SO_4$ were measured for each membrane sample and are presented in Fig. 5, along with the temporal evolution of $R_m$ that has been shown in

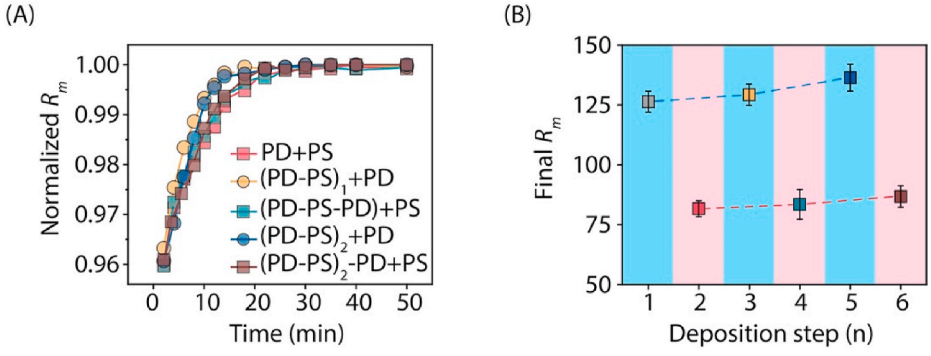


**Fig. 4. (A)** Temporal evolution of $R_m$ in different deposition steps, with squares representing PS adsorption onto a PD-coated surface and circle representing PD adsorption onto a PS-coated surface) **(B)** Final $R_m$ (i.e., $R_m$ at the end of each adsorption step). for each deposition step.

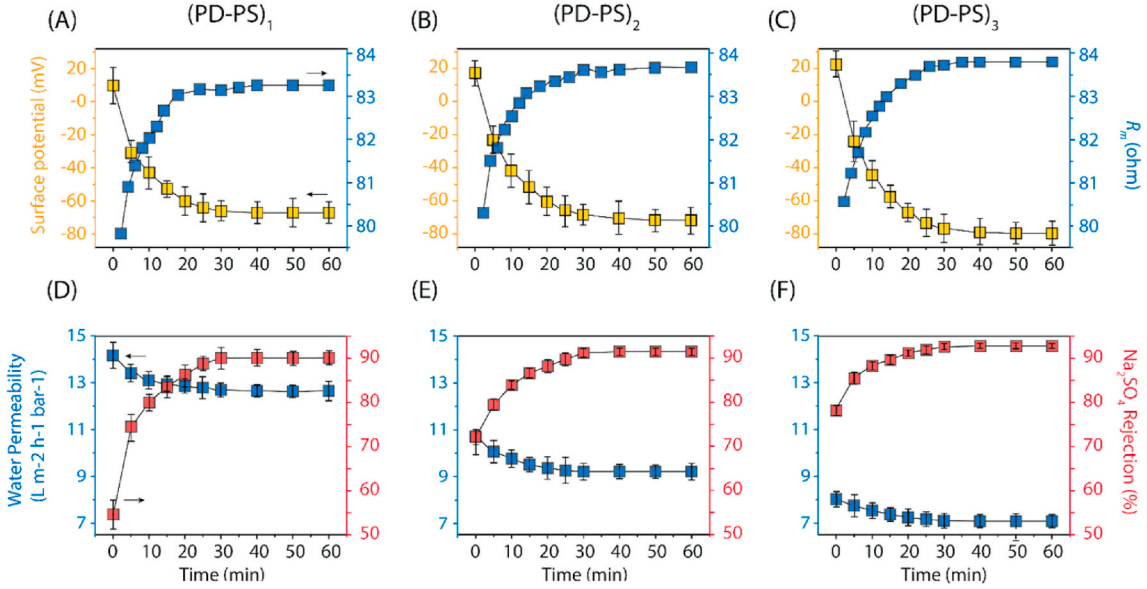


**Fig. 5.** **(A, B, C)** Surface streaming potential (orange squares, left axis), $R_m$ at a different time of the adsorption(green squares, right axis). **(D, E, F)** Membrane water permeability (blue squares, bottom row, left axis), and $Na_2SO_4$ rejection (red squares, bottom row, right axis) for PEM-NF membranes fabricated using different deposition time. All four sets of data are presented for PEM-NF membranes with one bilayer (PD-PS, first column), two bilayers ($(PD-PS)_2$, second column), and three bilayers of ($(PD-PS)_3$, third column).

Fig. 4A also presented in Fig. 5A, B and 5C to facilitate comparison.

Regardless of the number of PD-PS bilayers, the surface potential of the PEM-NF membranes as a function of adsorption time followed the opposite trend for the temporal evolution of $R_m$. As the EIS data in Fig. 3 suggests, the polyelectrolyte deposition completed at ~30 min. This is again confirmed by the temporal evolution of surface potential that reached its minimum at ~30 min. Similar behaviors were also observed with the membrane performance. Specifically, the water permeability decreased, and the salt rejection increased, with increasing deposition time, before they leveled off at ~30 min, which is in a good agreement with the change of $R_m$ (Fig. 5). These evidences are congruent in supporting the conclusion that ~30 min is required for this specific PEM system to reach completion of each deposition step (i.e., reaching an adsorption equilibrium beyond which membrane properties no longer change).

The validation of the hypothesis derived from EIS measurement suggests that we can indeed use data from a single EIS measurement to determine the extent of the deposition as a function of the deposition time. However, EIS measurement is substantially more convenient and efficient as compared to all the other measurements of membrane property or performance. For example, constructing each surface potential curve in Fig. 5A, B, and C requires the fabrication of ten membrane samples and at least ten surface potential measurements (even without replicate). The same number of membrane samples and measurements are also required for constructing the permeability and rejection curves in Fig. 5D, E, and F. All these series of measurements are time-consuming and laborious due to the requirements of fabricating multiple membranes and performing separate experiments on different membrane samples. In many cases when a membrane with the highest rejection is of primary interest, one can simply perform a single EIS measurement to identify the minimum deposition time for reaching surface saturation.

The EIS measurements do not only provide insights into the dynamics of polyelectrolyte adsorption in each step of LbL deposition, the film resistance of the membrane also correlates with the membrane performance such as water permeance and solute rejection. Specifically, this film resistances, $R_m$, were extracted from the EIS spectra at the end of each deposition step (i.e., the final points of $R_m$ in Fig. 5A, B, and C). As discussed before, $R_m$ quantifies the resistance of ion transport through the PEM layer and is dependent on both film thickness and surface charge. The small difference between $R_m$ of the three PS-capped PEMs, which was nonetheless detectable by the four-electrode EIS setup, led to substantial variation of water permeability and $Na_2SO_4$ rejection of the resulting NF membranes (Fig. 6). Specifically, $Na_2SO_4$ rejection increases with increasing $R_m$, as more difficult ion transport results in higher salt rejection; whereas water permeability decreases substantially with increasing $R_m$, primarily due to the increase of PEM film thickness.

## 4. Conclusion

In summary, we have developed a novel approach for in-situ and non-destructive monitoring of the adsorption kinetics of polyelectrolytes in the process of fabricating PEM-NF membranes using LbL deposition. The four-electrode EIS system is capable of detecting subtle electrochemical change of the properties in the solution near the membrane surface (interfacial solution resistance) and in the PEM layer (film resistance). The measurements of these properties in the adsorption process can reflect status of the adsorption process. Moreover, the film resistance extracted from EIS also correlates with the NF performance of

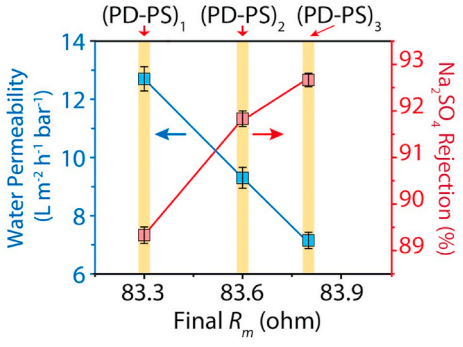


**Fig. 6.** Dependence of water permeability and $Na_2SO_4$ rejection on film resistance, $R_m$, extracted from the EIS spectrum at the end of each deposition step for PS-capped PEM. Such an $R_m$ was measured when polyelectrolyte adsorption reached equilibrium.

the PEM membrane.

Although the EIS technique cannot provides spatial distribution of the PEM properties, the ability to in-situ monitor global kinetics of the dynamic growth of the polyelectrolyte thin film has substantial practical implications for fabricating NF membranes using LbL deposition of polyelectrolytes. One obvious application of this EIS-based monitoring technique, as shown in this study, is to identify the minimum adsorption time to achieve surface saturation, which is critical for achieving the most efficient fabrication without compromising membrane performance. This technique may also help us better understand how the kinetics of polyelectrolyte deposition and membrane performance are affected by fabrication conditions such as temperature, pH, ionic strength, and the addition of solvents. Specifically, the dynamic information extracted from EIS can provide fundamental insights that cannot be derived from merely testing the performance of the fabricated membrane. Last but not least, this EIS-based monitoring approach applies not only to NF membrane fabrication, but also to any process of modifying membrane surfaces and many other substrate surfaces with polyelectrolyte adsorption.

## CRediT authorship contribution statement

**Yuanzhe Liang:** Data analysis, visualization, writing - original draft. **Fei Gao:** Data analysis, writing - original draft. **Li Wang:** Data analysis, writing - review & editing. **Shihong Lin:** Conceptualization, writing - review & editing.

## Declaration of competing interest

The authors declare no competing financial interest.

## Acknowledgment

The authors acknowledge the support from the Desalination and Water Purification Research Program of the US Bureau of Reclamation (R18AC00110) and National Science Foundation (1739884). F.G. also acknowledges the support from the China Scholarship Council (201806250113).

## Appendix A. Supplementary data

Supplementary data to this article can be found online at https://doi.org/10.1016/j.memsci.2020.118747.

## References

[1] C.M. Galanakis, G. Fountoulis, V. Gekas, Nanofiltration of brackish groundwater by using a polypiperazine membrane, Desalination 286 (2012) 277–284.
[2] Z. Wang, Z. Wang, S. Lin, H. Jin, S. Gao, Y. Zhu, J. Jin, Nanoparticle-templated nanofiltration membranes for ultrahigh performance desalination, Nat. Commun. 9 (2018) 1–36, https://doi.org/10.1038/s41467-018-04467-3.
[3] J.L. Acero, F.J. Benitez, A.I. Leal, F.J. Real, F. Teva, Membrane filtration technologies applied to municipal secondary effluents for potential reuse, J. Hazard Mater. 177 (2010) 390–398.
[4] W.-J. Lau, A.F. Ismail, Polymeric nanofiltration membranes for textile dye wastewater treatment: preparation, performance evaluation, transport modelling, and fouling control-a review, Desalination 245 (2009) 321–348.
[5] S. Yang, J. Wang, L. Fang, H. Lin, F. Liu, C.Y. Tang, Electrosprayed polyamide nanofiltration membrane with intercalated structure for controllable structure manipulation and enhanced separation performance, J. Membr. Sci. 602 (2020) 117971.
[6] G. Han, T.-S. Chung, M. Weber, C. Maletzko, Low-pressure nanofiltration hollow fiber membranes for effective fractionation of dyes and inorganic salts in textile wastewater, Environ. Sci. Technol. 52 (2018) 3676–3684.
[7] C. Boo, Y. Wang, I. Zucker, Y. Choo, C.O. Osuji, M. Elimelech, High performance nanofiltration membrane for effective removal of perfluoroalkyl substances at high water recovery, Environ. Sci. Technol. 52 (2018) 7279–7288.
[8] A.W. Mohammad, Y.H. Teow, W.L. Ang, Y.T. Chung, D.L. Oatley-Radcliffe, N. Hilal, Nanofiltration membranes review: recent advances and future prospects, Desalination 356 (2015) 226–254, https://doi.org/10.1016/j.desal.2014.10.043.
[9] Y. Liang, Y. Zhu, C. Liu, K.-R. Lee, W.-S. Hung, Z. Wang, Y. Li, M. Elimelech, J. Jin, S. Lin, Polyamide nanofiltration membrane with highly uniform sub-nanometre pores for sub-1A precision separation, Nat. Commun. 11 (2020) 1–9.
[10] X. Zhu, X. Cheng, X. Luo, Y. Liu, D. Xu, X. Tang, Z. Gan, L. Yang, G. Li, H. Liang, Ultrathin thin-film composite polyamide membranes constructed on hydrophilic poly (vinyl alcohol) decorated support toward enhanced nanofiltration performance, Environ. Sci. Technol. 54 (2020) 6365–6374.
[11] A.E. Childress, M. Elimelech, Relating nanofiltration membrane performance to membrane charge (electrokinetic) characteristics, Environ. Sci. Technol. 34 (2000) 3710–3716.
[12] H. Zhang, X. Quan, X. Fan, G. Yi, S. Chen, H. Yu, Y. Chen, Improving ion rejection of conductive nanofiltration membrane through electrically enhanced surface charge density, Environ. Sci. Technol. 53 (2018) 868–877.
[13] R. Epsztein, E. Shaulsky, N. Dizge, D.M. Warsinger, M. Elimelech, Role of ionic charge density in donnan exclusion of monovalent anions by nanofiltration, Environ. Sci. Technol. 52 (2018) 4108–4116, https://doi.org/10.1021/acs.est.7b06400.
[14] J. Wang, D.S. Dlamini, A.K. Mishra, M.T.M. Pendergast, M.C.Y. Wong, B.B. Mamba, V. Freger, A.R.D. Verliefde, E.M.V. Hoek, A critical review of transport through osmotic membranes, J. Membr. Sci. 454 (2014) 516–537, https://doi.org/10.1016/j.memsci.2013.12.034.
[15] Q. Li, M. Elimelech, Organic fouling and chemical cleaning of nanofiltration membranes: measurements and mechanisms, Environ. Sci. Technol. 38 (2004) 4683–4693, https://doi.org/10.1021/es0354162.
[16] N. Hilal, N.A. Darwish, A.W. Mohammad, M.A. Arabi, A comprehensive review of nanofiltration membranes : treatment , pretreatment , modelling, and atomic force microscopy 170 (2004) 281–308, https://doi.org/10.1016/j.desal.2004.01.007.
[17] M. Paul, S.D. Jons, Chemistry and fabrication of polymeric nanofiltration membranes: a review, Polymer 103 (2016) 417–456, https://doi.org/10.1016/j.polymer.2016.07.085.
[18] S. Lin, Energy efficiency of desalination: fundamental insights from intuitive interpretation, Environ. Sci. Technol. (2020), https://doi.org/10.1021/acs.est.9b04788.
[19] J.J. Richardson, M. Björnmalm, F. Caruso, Technology-driven layer-by-layer assembly of nanofilms, Science 80– (2015) 348, https://doi.org/10.1126/science.aaa2491.
[20] J.J. Richardson, J. Cui, M. Björnmalm, J.A. Braunger, H. Ejima, F. Caruso, Innovation in layer-by-layer assembly, Chem. Rev. 116 (2016) 14828–14867, https://doi.org/10.1021/acs.chemrev.6b00627.
[21] M. Wang, Z. Wang, X. Wang, S. Wang, W. Ding, C. Gao, Layer-by-layer assembly of aquaporin Z-incorporated biomimetic membranes for water purification, Environ. Sci. Technol. 49 (2015) 3761–3768.
[22] Y. Zhu, M. Ahmad, L. Yang, M. Misovich, A. Yaroshchuk, M.L. Bruening, Adsorption of polyelectrolyte multilayers imparts high monovalent/divalent cation selectivity to aliphatic polyamide cation-exchange membranes, J. Membr. Sci. 537 (2017) 177–185.
[23] M. Ahmad, C. Tang, L. Yang, A. Yaroshchuk, M.L. Bruening, Layer-by-layer modification of aliphatic polyamide anion-exchange membranes to increase Cl-/SO42- selectivity, J. Membr. Sci. 578 (2019) 209–219.
[24] R.M. DuChanois, R. Epsztein, J.A. Trivedi, M. Elimelech, Controlling pore structure of polyelectrolyte multilayer nanofiltration membranes by tuning polyelectrolyte-salt interactions, J. Membr. Sci. 581 (2019) 413–420, https://doi.org/10.1016/j.memsci.2019.03.077.
[25] K.L. Cho, A.J. Hill, F. Caruso, S.E. Kentish, Chlorine resistant glutaraldehyde crosslinked polyelectrolyte multilayer membranes for desalination, Adv. Mater. 27 (2015) 2791–2796.
[26] L. Wang, N. Wang, J. Li, J. Li, W. Bian, S. Ji, Layer-by-layer self-assembly of polycation/GO nanofiltration membrane with enhanced stability and fouling resistance, Separ. Purif. Technol. 160 (2016) 123–131.
[27] E. Virga, J. de Grooth, K.Z. vab, W.M. de Vos, Stable polyelectrolyte multilayer-based hollow fiber nanofiltration membranes for produced water treatment, ACS Appl. Polym. Mater. 1 (2019) 2230–2239.
[28] S.U. Hong, R. Malaisamy, M.L. Bruening, Separation of fluoride from other monovalent anions using multilayer polyelectrolyte nanofiltration membranes, Langmuir 23 (2007) 1716–1722.
[29] J.B. Schlenoff, S.T. Dubas, Mechanism of polyelectrolyte multilayer growth: charge overcompensation and distribution, Macromolecules 34 (2001) 592–598, https://doi.org/10.1021/ma0003093.
[30] L. Shan, Y. Liang, L. Prozorovska, G.K. Jennings, S. Ji, S. Lin, Multifold enhancement of loose nanofiltration membrane performance by intercalation of surfactant assemblies, Environ. Sci. Technol. Lett. 5 (2018) 668–674, https://doi.org/10.1021/acs.estlett.8b00430.
[31] S.T. Dubas, J.B. Schlenoff, Factors controlling the growth of polyelectrolyte multilayers, Macromolecules 32 (1999) 8153–8160, https://doi.org/10.1021/ma981927a.
[32] C. Picart, J. Mutterer, L. Richert, Y. Luo, G.D. Prestwich, P. Schaaf, J.-C. Voegel, P. Lavalle, Molecular basis for the explanation of the exponential growth of polyelectrolyte multilayers, Proc. Natl. Acad. Sci. Unit. States Am. 99 (2002) 12531–12535.
[33] C. Porcel, P. Lavalle, V. Ball, G. Decher, B. Senger, J.-C. Voegel, P. Schaaf, From exponential to linear growth in polyelectrolyte multilayers, Langmuir 22 (2006) 4376–4383.
[34] B. Schoeler, G. Kumaraswamy, F. Caruso, Investigation of the influence of polyelectrolyte charge density on the growth of multilayer thin films prepared by the layer-by-layer technique, Macromolecules 35 (2002) 889–897, https://doi.org/10.1021/ma011349p.

[35] G. Decher, J.D. Hong, J. Schmitt, Buildup of ultrathin multilayer films by a self-assembly process: III. Consecutively alternating adsorption of anionic and cationic polyelectrolytes on charged surfaces, Thin Solid Films (1992) 831–835, https://doi.org/10.1016/0040-6090(92)90417-A, 210–211.
[36] Y. Hu, C. Neil, B. Lee, Y.-S. Jun, Control of heterogeneous Fe (III)(hydr) oxide nucleation and growth by interfacial energies and local saturations, Environ. Sci. Technol. 47 (2013) 9198–9206.
[37] M. Norgren, L. Gärdlund, S.M. Notley, M. Htun, L. Wågberg, Smooth model surfaces from lignin derivatives. II. adsorption of polyelectrolytes and PECs monitored by QCM-D, Langmuir 23 (2007) 3737–3743, https://doi.org/10.1021/la063439z.
[38] A.E. Contreras, Z. Steiner, J. Miao, R. Kasher, Q. Li, Studying the role of common membrane surface functionalities on adsorption and cleaning of organic foulants using QCM-D, Environ. Sci. Technol. 45 (2011) 6309–6315.
[39] B.C. Bonekamp, J. Lyklema, Conductometric and potentiometric monitoring of polyelectrolyte adsorption on charged surfaces, J. Colloid Interface Sci. 113 (1986) 67–75, https://doi.org/10.1016/0021-9797(86)90206-7.
[40] A. Poghossian, M.H. Abouzar, M. Sakkari, T. Kassab, Y. Han, S. Ingebrandt, A. Offenhäusser, M.J. Schöning, Field-effect sensors for monitoring the layer-by-layer adsorption of charged macromolecules, Sensor. Actuator. B Chem. 118 (2006) 163–170, https://doi.org/10.1016/j.snb.2006.04.013.
[41] K. Jüttner, Electrochemical impedance spectroscopy (EIS) of corrosion processes on inhomogeneous surfaces, Electrochim. Acta 35 (1990) 1501–1508, https://doi.org/10.1016/0013-4686(90)80004-8.
[42] F. Mansfeld, Use of electrochemical impedance spectroscopy for the study of corrosion protection by polymer coatings, J. Appl. Electrochem. 25 (1995) 187–202, https://doi.org/10.1007/BF00262955.
[43] W.F. Chen, C.H. Wang, K. Sasaki, N. Marinkovic, W. Xu, J.T. Muckerman, Y. Zhu, R.R. Adzic, Highly active and durable nanostructured molybdenum carbide electrocatalysts for hydrogen production, Energy Environ. Sci. 6 (2013) 943–951, https://doi.org/10.1039/c2ee23891h.
[44] H.-K. Song, Y.-H. Jung, K.-H. Lee, L.H. Dao, Electrochemical impedance spectroscopy of porous electrodes: the effect of pore size distribution, Electrochim. Acta 44 (1999) 3513–3519, https://doi.org/10.1016/S0013-4686(99)00121-8.
[45] S.V.P. Barreira, V. García-Morales, C.M. Pereira, J.A. Manzanares, F. Silva, Electrochemical impedance spectroscopy of polyelectrolyte multilayer modified electrodes, J. Phys. Chem. B 108 (2004) 17973–17982, https://doi.org/10.1021/jp0466845.
[46] M. Chirea, V. García-Morales, J.A. Manzanares, C. Pereira, R. Gulaboski, F. Silva, Electrochemical characterization of polyelectrolyte/gold nanoparticle multilayers self-assembled on gold electrodes, J. Phys. Chem. B 109 (2005) 21808–21817, https://doi.org/10.1021/jp0537815.
[47] W. Cheng, C. Liu, T. Tong, R. Epsztein, M. Sun, R. Verduzco, J. Ma, M. Elimelech, Selective removal of divalent cations by polyelectrolyte multilayer nanofiltration membrane: role of polyelectrolyte charge, ion size, and ionic strength, J. Membr. Sci. 559 (2018) 98–106, https://doi.org/10.1016/j.memsci.2018.04.052.
[48] M. Grossi, B. Riccò, Electrical impedance spectroscopy (EIS) for biological analysis and food characterization: a review, J. Sensors Sens. Syst. 6 (2017) 303–325, https://doi.org/10.5194/jsss-6-303-2017.
[49] S. Bason, Y. Oren, V. Freger, Characterization of ion transport in thin films using electrochemical impedance spectroscopy. II: examination of the polyamide layer of RO membranes, J. Membr. Sci. 302 (2007) 10–19, https://doi.org/10.1016/j.memsci.2007.05.007.
[50] D.-J. Yun, H. Ra, S.-W. Rhee, Concentration effect of multiwalled carbon nanotube and poly (3, 4-ethylenedioxythiophene) polymerized with poly (4-styrenesulfonate) conjugated film on the catalytic activity for counter electrode in dye sensitized solar cells, Renew. Energy 50 (2013) 692–700.
[51] M. Stolov, V. Freger, Degradation of polyamide membranes exposed to chlorine: an impedance spectroscopy study, Environ. Sci. Technol. 53 (2019) 2618–2625.
[52] V. Freger, S. Bason, Characterization of ion transport in thin films using electrochemical impedance spectroscopy. I. Principles and theory, J. Membr. Sci. 302 (2007) 1–9, https://doi.org/10.1016/j.memsci.2007.06.046.
[53] M. Stolov, V. Freger, Membrane charge weakly affects ion transport in reverse osmosis, Environ. Sci. Technol. Lett. 7 (2020) 440–445, https://doi.org/10.1021/acs.estlett.0c00291.
[54] N. Fridman-Bishop, V. Freger, What makes aromatic polyamide membranes superior: new insights into ion transport and membrane structure, J. Membr. Sci. 540 (2017) 120–128, https://doi.org/10.1016/j.memsci.2017.06.035.
[55] D.L. Shaffer, K.E. Feldman, E.P. Chan, G.R. Stafford, C.M. Stafford, Characterizing salt permeability in polyamide desalination membranes using electrochemical impedance spectroscopy, J. Membr. Sci. 583 (2019) 248–257.
[56] O. Squillace, C. Esnault, J.-F. Pilard, G. Brotons, Electrodes for membrane surface science. Bilayer lipid membranes tethered by commercial surfactants on electrochemical sensors, ACS Sens. 4 (2019) 1337–1345.
[57] A. V Delgado, F. Gonzalez-Caballero, R.J. Hunter, L.K. Koopal, J. Lyklema, Measurement and interpretation of electrokinetic phenomena, J. Colloid Interface Sci. 309 (2007) 194–224.
[58] A. Yaroshchuk, T. Luxbacher, Interpretation of electrokinetic measurements with porous films: role of electric conductance and streaming current within porous structure, Langmuir 26 (2010) 10882–10889.
[59] P. Fievet, M. Sba, A. Szymczyk, A. Vidonne, Determining the -potential of plane membranes from tangential streaming potential measurements: effect of the membrane body conductance, J. Membr. Sci. 226 (2003) 227–236.
[60] M. Sbai, A. Szymczyk, P. Fievet, A. Sorin, A. Vidonne, S. Pellet-Rostaing, A. Favre-Reguillon, M. Lemaire, Influence of the membrane pore conductance on tangential streaming potential, Langmuir 19 (2003) 8867–8871.
[61] P. Nestler, M. Paßvogel, C.A. Helm, Influence of polymer molecular weight on the parabolic and linear growth regime of PDADMAC/PSS multilayers, Macromolecules 46 (2013) 5622–5629, https://doi.org/10.1021/ma400333f.
[62] E. Guzmun, H. Ritacco, J.E.F. Rubio, R.G. Rubio, F. Ortega, Salt-induced changes in the growth of polyelectrolyte layers of poly (diallyl-dimethylammonium chloride) and poly (4-styrene sulfonate of sodium), Soft Matter 5 (2009) 2130–2142.
[63] C. Kleber, M. Bruns, K. Lienkamp, J. Ruhe, M. Asplund, An interpenetrating, microstructurable and covalently attached conducting polymer hydrogel for neural interfaces, Acta Biomater. 58 (2017) 365–375.
[64] I. Teraoka, Polymer Solutions, John Wiley & Sons, Inc, 2002.
[65] C.M. Kok, A. Rudin, Relationship between the hydrodynamic radius and the radius of gyration of a polymer in solution, Makromol. Chem. Rapid Commun. 2 (1981) 655–659.
[66] E.R. Nightingale Jr., Phenomenological theory of ion solvation. Effective radii of hydrated ions, J. Phys. Chem. 63 (1959) 1381–1387.